

Probing higher-order corrections in dijet production at the LHC

Simone Alioli

*Ernest Orlando Lawrence Berkeley National Laboratory, University of California,
Berkeley, CA 94720, USA
E-mail: salioli@lbl.gov*

Jeppe R. Andersen

*CP³-Origins, University of Southern Denmark, Campusvej 55,
DK-5230 Odense M, Denmark
E-mail: jeppe.andersen@cern.ch*

Carlo Oleari

*Università di Milano-Bicocca and INFN, Sezione di Milano-Bicocca
Piazza della Scienza 3, 20126 Milan, Italy
E-mail: carlo.oleari@mib.infn.it*

Emanuele Re

*IPPP, Department of Physics, University of Durham, Durham, DH1 3LE, UK
E-mail: emanuele.re@durham.ac.uk*

Jennifer M. Smillie

*School of Physics and Astronomy, University of Edinburgh, Mayfield Road, Edinburgh
EH9 3JZ, UK
E-mail: j.m.smillie@ed.ac.uk*

ABSTRACT: We discuss the comparisons of several kinematic distributions, measured by the ATLAS and CMS Collaborations for dijet production, with the results computed with three approaches: using a fixed next-to-leading order calculation, with the POWHEG BOX and with HEJ. We study other interesting kinematic distributions, exploring the effect of several sets of cuts. Previous experimental studies have dealt with kinematic distributions where the predictions of the three approaches were very similar. In this article, we investigate kinematic distributions where the resummed effects in POWHEG and HEJ are enhanced with respect to the fixed next-to-leading order result, since different QCD-radiation regimes are probed, and we suggest a few kinematic distributions where the predictions from POWHEG and HEJ are different, and could be further investigated experimentally.

KEYWORDS: QCD, Monte Carlo, NLO Computations, Resummation, Collider Physics.

Contents

1. Introduction	1
2. Dijet production at the LHC	3
2.1 ATLAS results	3
2.2 CMS results	5
2.3 Summary	5
3. Reliability of the NLO predictions	6
4. Probing higher-order corrections: a comparison among POWHEG, HEJ and NLO results	9
5. Conclusions	14

1. Introduction

Dijet production is one of the cornerstone processes at the LHC. The cross section for jet production is very large, making it an important testing ground for our understanding of QCD at high-energy scales. In addition, jet production is an important background for many searches for new physics. It is therefore essential to probe and test our theoretical predictions.

Dijet production is not only important by itself but also when the jets are accompanying other particles, such as the W/Z vector bosons or the Higgs boson. For example, Higgs boson production plus two jets is an important process in the Standard Model (SM). Two different processes have Hjj as final-state signature: in the first one, the Higgs boson couples to gluons via a top-quark loop [1, 2], while in the second one, the Higgs boson is produced by vector-boson fusion (VBF) [3, 4, 5], stemming from two incoming quarks. The vector-boson fusion process is particularly important to extract the HWW and HZZ couplings, and to confirm if the detected Higgs boson is the scalar responsible for the electroweak symmetry breaking. In addition, information on the CP properties of the Higgs boson can be extracted by studying the azimuthal distributions of the two hardest jets [6, 7], in events with a large ($\gtrsim 3$ units) rapidity separation between them. In fact, the signature of the VBF Higgs boson production are two jets well separated in rapidity. In addition, we expect very low hadronic activity between the two hardest jets, due to the exchange of the colorless vector bosons in the t channel [8], on the contrary of what is expected for the gluon-fusion production mechanism. A key feature is then the study of the efficiency of the central-jet veto, to suppress gluon-fusion processes [1, 2], where it is

well known that the higher-order corrections [9, 10, 11, 12] are very significant [13], and a detailed understanding [14, 15, 16, 17] of the structure of the radiation pattern is needed.

Some of the features in Hjj production in gluon fusion are in fact universal [13] to dijet processes in general, like $W/Z + 2$ jets or pure dijet production, and may help as a testing ground for techniques which can be applied in the Higgs boson searches and studies. Before the possible study of processes with a Higgs boson, it thus becomes interesting to investigate the (hard) radiation pattern in events with at least two jets, in particular for events with a non-negligible rapidity separation between the two jets. The central question is whether a framework based on a (possibly next-to-leading-order-matched) parton shower (which resums the radiation resulting from a large ratio in transverse scales) is sufficient for the description of additional jets, or whether BFKL-type [18, 19, 20, 21] effects from hard, wide-angle emissions, have already become important at the center of mass energy of the LHC (currently 7 TeV).

In light of this, there have been a number of very interesting experimental studies in dijet production by both the ATLAS [22, 23, 24] and CMS [25, 26, 27] Collaborations. It is already clear that higher-order QCD contributions, beyond a fixed order, low multiplicity calculation, can be important, because the large available phase space for jet emission at the LHC compensates for the suppression of extra powers in the strong coupling constant.

In this paper, we compare two theoretical approaches to dijet production, that include higher order effects: **POWHEG** [28, 29, 30] and **HEJ** [31, 32, 33]. The **POWHEG** method successfully merges a fixed next-to-leading order (NLO) calculation with a parton shower program, that resums leading logarithmic contributions from collinear emissions. In this study, the **POWHEG** results obtained with the **POWHEG BOX** [34] are interfaced with the transverse-momentum-ordered shower provided by **PYTHIA 6.4.25** [35]. In contrast, the starting point for **HEJ** (High Energy Jets) is an all-order approximation to the hard scattering matrix element in the regime of wide-angle QCD emissions. **HEJ** is accurate at leading logarithmic precision in the invariant mass of any two jets. This is then supplemented with the missing contributions (through a merging and reweighting procedure) necessary to also ensure tree-level accuracy for final states with up to four jets. The tree-level matrix elements are taken from Standalone Madgraph [36].

The layout of the paper is the following: in section 2 we discuss in detail existing experimental analyses and theoretical predictions. Since our goal is to compare the **POWHEG** and **HEJ** approaches to the fixed NLO results too, in section 3 we study several sets of cuts, that do not induce a large hierarchy in the transverse scales but impose a large rapidity separation between the jets, and we investigate for which set the NLO results remain reliable and do not suffer from large unresummed logarithmic terms, due to incomplete cancellation of virtual contributions [37, 38, 39, 30]. In section 4, we investigate and propose a few analyses which will better expose the differences between **POWHEG** and **HEJ**, and will allow us to better understand which is the dominant mechanism in the generation of radiation. Finally, we summarize our findings in section 5.

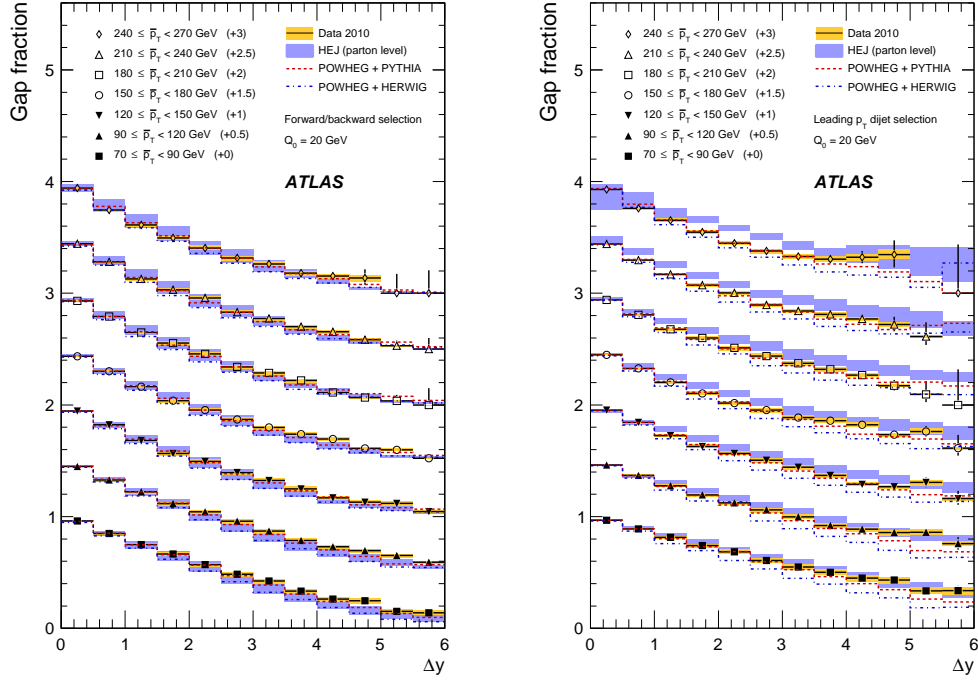


Figure 1: Both plots from the ATLAS study [22] on the gap fraction, defined as the fraction of events with no additional jets in the rapidity region between the tagging jets, as a function of the difference of the rapidity of the two jets. In the left-hand side plot, the tagging jets are the most forward and most backward jet, while in the right-hand side plot, they are the two hardest jets in each event. In both plots, \bar{p}_T is the average transverse momentum of two tagging jets. All jets are required to have $p_T > 20$ GeV and absolute rapidity $|y| < 4.4$.

2. Dijet production at the LHC

In this section, we discuss in detail existing experimental analyses where dijet data collected by ATLAS and CMS have been compared with the theoretical results obtained with the POWHEG BOX and HEJ. The POWHEG and HEJ approaches are clearly very different in their description of QCD radiation: one approach resums collinear emissions while the other soft and hard, wide-angle emissions. Nevertheless, for several kinematic distributions (see for example ref. [22]) the predictions from POWHEG and HEJ are very similar. This is due, as we show in this section, to the inclusiveness of the studied kinematic distributions and on the values of the cuts applied in the experimental analysis.

2.1 ATLAS results

Among several dijet results published by the ATLAS Collaboration, one is of particular interest to us: a study of the production of additional jets from a dijet system [22]. In this study, jets are reconstructed using the anti- k_T jet algorithm [40] with $R = 0.6$ and required to have a transverse momentum above 20 GeV, with absolute rapidity less than 4.4. We show in fig. 1 extracts from this ATLAS study, where the gap fraction, defined as the fraction of events with no additional jets in the rapidity region between the two tagging

jets, is plotted as a function of Δy , the difference of the rapidities of two tagging jets. In the left plot, the tagging jets are defined to be the most forward and most backward jet (in rapidity), while, in the right plot, they are chosen to be the two hardest jets (highest transverse momentum) in each event. In both plots, \bar{p}_T is the average transverse momentum of two tagging jets, and results are shown for slices of the average transverse momentum \bar{p}_T ranging from 70 GeV up to 500 GeV. The experimental data is then compared with the predictions from HEJ (the blue band indicating the scale variation obtained by varying the (equal) renormalization and factorization scale by a factor of two), and the POWHEG predictions showered by PYTHIA and HERWIG.

We would like to add a few comments to these findings:

1. In the left plot, the theoretical predictions obtained in the two very different approaches of HEJ and POWHEG are very similar, and agree with data over a wide range of rapidity intervals and average transverse-momentum slices. For this kinematic quantity, where the tagging jets are selected to be the forward/backward ones, a large hierarchy in the transverse momenta of these jets develops as the average transverse momentum of the forward/backward jets is increased, so that at least one of the forward/backward jets must be very hard. Indeed, it is observed that for this selection, the average difference in the transverse momentum of the forward/backward jet increases systematically with increasing Δy . Since the veto scale (Q_0 in the label of the figure) for counting additional jets is much smaller than the average transverse momentum of the tagging jets, the jet production is driven by relatively-soft emission from the dijet system. Both HEJ and POWHEG, with different approximations, do include these multiple emissions giving a good agreement with data.
2. In the right plot of fig. 1, where the tagging jets are chosen to be the two hardest jets in the event, as the average p_T of the two hardest jets increases to 5 times or more of the veto scale Q_0 , the HEJ prediction starts deviating from data, underestimating the amount of radiation (i.e. the prediction for the gap fraction is larger than the data). This behavior is expected, since the component of events added with naïve tree-level matching increases with increasing \bar{p}_T . This component receives no systematic treatment of soft resummation within HEJ, a situation which would be improved by a complete matching with a parton shower. Progress in this direction has recently been made in ref. [41].

The POWHEG description includes the effects of collinear emissions through the shower formulations, and the theoretical predictions perform well for both the two kinematic distributions in fig. 1 (particularly when using the PYTHIA shower). However, as can be seen in the right plot, for larger rapidity spans and modest \bar{p}_T , the POWHEG description undershoots the data. Indeed, POWHEG contains no systematic resummation of all the leading logarithmic terms for large Δy . Overall, the study reported by ATLAS shows best agreement with the predictions of POWHEG+PYTHIA, but all the studies involve a hierarchy of transverse scales, and therefore, by construction, will favor the description with the systematic collinear resummation of a parton shower.

Note that the results for POWHEG+HERWIG are consistently below data (i.e. the events contain too many jets). The differences between the results from POWHEG+PYTHIA and POWHEG+HERWIG should be considered as a theoretical uncertainty connected to the different shower algorithm.

As a final comment, we are interested in separating the two mechanisms for creating additional jet activity, i.e. a hierarchy of transverse scales (as in the POWHEG shower), and the opening of phase space as the rapidity span between two jets is increased (as in HEJ). For this separation to take place, it is obviously necessary to introduce a selection criteria which does not automatically generate a hierarchy in the transverse scales as the rapidity span increases. This is partially done in the study performed by the CMS Collaboration, discussed in the following section.

2.2 CMS results

CMS has reported a study [27] on dijet production with just a simple selection criteria on the transverse momenta of jets. Jets are reconstructed using the anti- k_T algorithm with $R = 0.5$, and are requested to have $p_T > 35$ GeV. Events are then required to contain at least one forward jet ($3.2 < |\eta^f| < 4.7$) and at least one central jet ($|\eta^c| < 2.8$), where η is the pseudorapidity of the jets. The transverse-momentum spectrum of the hardest central and hardest forward jet is then studied. Obviously, any difference in the two spectra is a result of radiation beyond the tree-level description of back-to-back partons. While the CMS study extends the pseudo-rapidity region of jets up to 4.7 units, the transverse momentum distributions are integrated over these pseudo-rapidity ranges. Crucially, however, no large p_T -hierarchy is induced by the cuts, and this gives a cleaner study of the separate effects of the relatively modest rapidity gap.

In the CMS analysis, HEJ describes the p_T -spectrum well for both the central and the forward jets. POWHEG+HERWIG describes the shape correctly, but the normalization is consistently high. The POWHEG+PYTHIA description of the forward jet p_T -distribution performs well, but the description for the central jet shows deviations in both shape and normalization. As the events in this analysis have been specifically selected to have a non-negligible rapidity span, this slight deviation could be attributed to the absence of a systematic treatment of the dominant logarithmic terms for increasing $\Delta\eta$.

2.3 Summary

The analyses discussed so far show that the descriptions of both POWHEG and HEJ are performing well, and in broad agreement. The close agreement between the two can, to some extent, be attributed to the requirement of a large p_T -hierarchy in the study by ATLAS, or the modest average rapidity spans in the study by CMS.

In the rest of this paper, we investigate various observables which can expose the differences among the fixed NLO calculation, the POWHEG and HEJ approaches. The first task is therefore to develop a set of cuts, for which the NLO prediction for dijet production is physically meaningful. This is the topic of the next section.

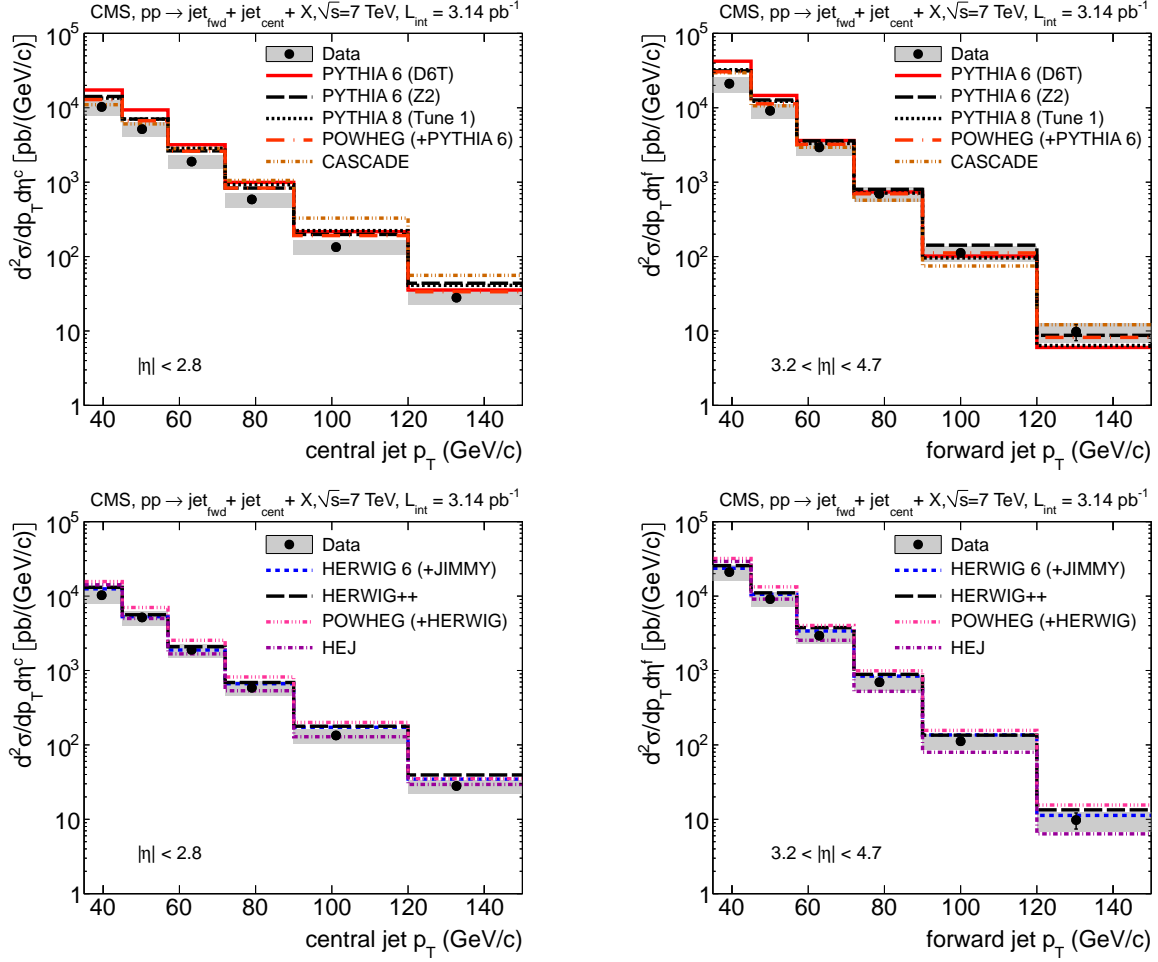


Figure 2: The transverse momentum distributions of the leading forward jet ($3.2 < |\eta^f| < 4.7$) and the leading central jet ($|\eta^c| < 2.8$) in a sample which requires at least one jet with $p_T > 35$ GeV in each region. The top and bottom row contain the same data points, but different theoretical predictions. The plots are taken from [27].

3. Reliability of the NLO predictions

It has been known for a while that fixed-order results for dijet production are not reliable when symmetric cuts are applied to the transverse momentum of the two hardest jets. This was first noticed in [42, 37], in the context of electron-proton collisions at HERA, and later also in hadron collisions [38]. A detailed theoretical discussion of the origin of this fact can be found in [39], where the next-to-leading logarithmic resummation of soft logarithms was also performed.

While the fixed-order theoretical predictions display an unphysical behavior as the symmetric-cut limit is reached, the experimental data are obviously not affected by that. If we are interested in a comparison of the fixed NLO result with data, then we have to impose asymmetric cuts

$$p_T^j > p_T^{\min}, \quad p_T^{j_1} > p_T^{\min} + \Delta p_T, \quad \Delta p_T > 0, \quad (3.1)$$

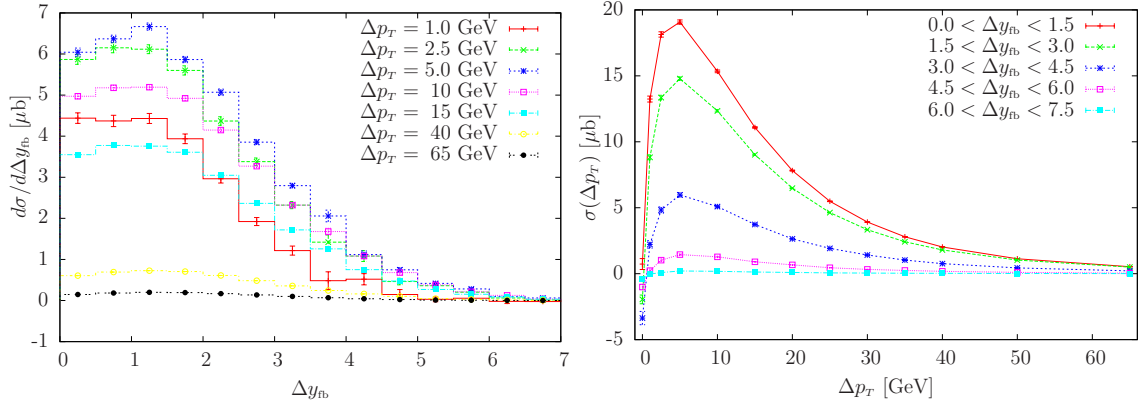


Figure 3: The dependence of the $d\sigma/d\Delta y_{fb}$ distribution on the asymmetry of jet cuts (left plot) and of the total cross section in different Δy_{fb} slices, as a function of the jet cuts asymmetry Δp_T (right plot).

i.e. all jets are required to have a minimum transverse momentum p_T^{\min} , while a stronger constraint is applied to the hardest jet in the event, with transverse momentum $p_T^{j_1}$. In our notation, Δp_T quantifies then the asymmetry on the cuts. Since in this paper we are interested in studying the size of QCD corrections in regions traditionally used to probe BFKL-like effects, we allow for quite forward jets. Therefore we impose the condition, $|y_j| < 4.7$, on the jet rapidities, and we set $p_T^{\min} = 35$ GeV (similar to the CMS cut discussed in the previous section). Jets are reconstructed using the anti- k_T jet algorithm [40] with $R = 0.5$ and default recombination scheme. The NLO results, as well as the POWHEG distributions shown in section 4, have been obtained with renormalization and factorization scales set to the POWHEG underlying-Born transverse momentum, i.e. the p_T of the partons in the Born-like $2 \rightarrow 2$ kinematics, starting point for the generation of radiation [30]. For all the plots in the paper we have used the MSTW2008 [43] parton distribution function set. The aim of this section is to explore several sets of cuts to be applied to the jets and to clarify the breaking-point, where the NLO calculation becomes unreliable.

In fig. 3 we illustrate the effects of the cuts of eq. (3.1): in the left plot, we display the differential cross section for dijet inclusive production as a function of Δy_{fb} , the difference in rapidity of the most forward and most backward jet. The various curves correspond to different values of Δp_T in eq. (3.1), ranging from $\Delta p_T = 1$ GeV up to $\Delta p_T = 65$ GeV. On physical grounds, we expect a decrease of the differential cross section as Δp_T increases. However, and as noted in earlier studies [30], we observe that the results do not show this behaviour. Indeed, over a wide range in Δy_{fb} , the cross sections increase for increasing Δp_T till a maximum is reached at $\Delta p_T \approx 5$ GeV. Then, for any further increase of Δp_T , the cross section decreases, as expected. This is caused by large logarithmic term in Δp_T , arising from a veto in the emission of radiation above the Δp_T scale, which causes uncanceled virtual corrections to build up above this scale. The same behaviour is also evident in the right plot of fig. 3, where the cross section is plotted against Δp_T for various slices in Δy_{fb} . The presence of uncanceled virtual corrections becomes manifest for small Δp_T , where the cross section is unphysically negative.

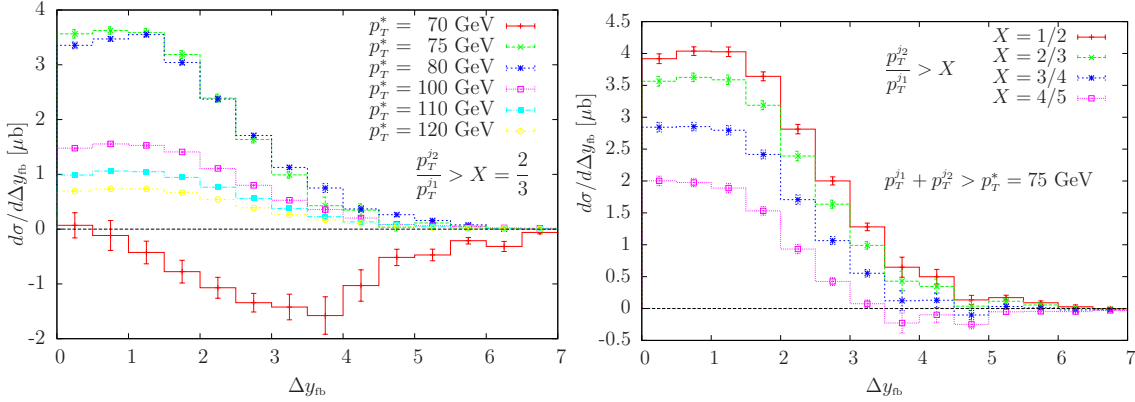


Figure 4: The differential cross sections $d\sigma/d\Delta y_{fb}$ for several values of p_T^* at $X = 2/3$ (left plot) and for several values of X for $p_T^* = 75$ GeV (right plot). For both plots, jets have transverse momentum greater than 35 GeV.

In fig. 4, we plot the differential cross section as a function of Δy_{fb} using another set of cuts, BFKL inspired:

$$p_T^j > p_T^{\min}, \quad p_T^{j_1} + p_T^{j_2} > p_T^*, \quad \frac{p_T^{j_2}}{p_T^{j_1}} > X, \quad |y_j| < 4.7, \quad (3.2)$$

where j_1 and j_2 denote the hardest and next-to-hardest jet. In the left plot of fig. 4, we show the cross sections obtained at a fixed value of X (chosen here to be $2/3$) for several values of p_T^* ¹. The rôle of Δp_T in fig. 3 is now played by the distance $p_T^* - 2p_T^{\min}$. In fact, when p_T^* reaches its minimum value equal to $2p_T^{\min}$, jets can approach the symmetric-cut configuration, exposing again large logarithms in a fixed NLO calculation. The red curve shows precisely the unphysical behavior when $p_T^* = 2p_T^{\min} = 70$ GeV, giving rise to a negative cross section. We have checked that this conclusion holds regardless of the value of X chosen. As p_T^* increases beyond its minimal value, the cross sections exhibit a physical behavior, i.e. they decrease. In the right plot of fig. 4, we display the differential cross sections for $p_T^* = 75$ GeV and for several values of X . The symmetric-cut regime is here reached when $X \rightarrow 1$, and in fact, as the values of X increases, the differential cross sections develop a negative tails for high Δy_{fb} .

The two plots in fig. 5, and similar ones that can be drawn for other values of X and p_T^* , can help in the not-easy task of establishing what cuts to apply in an analysis if one wants to compare the experimental data to the NLO calculation using the alternative cuts of eq. (3.2). In the left plot, the cross sections plotted for several slices in Δy_{fb} become negative for values of p_T^* less than 75 GeV, fixing then a lower value below which the theoretical distributions cannot be trusted. Similarly, the right plot, where the cross sections are plotted as a function of X at fixed value of $p_T^* = 75$ GeV, gives an indication of the upper value of X above which the NLO predictions become unreliable, for different slices of Δy_{fb} .

¹While in principle X can vary from 0 to 1, it can be shown that, for a partonic $2 \rightarrow n$ process, the lower limit is not 0, but $1/(n-1)$, so that, in our study ($n=3$), $1/2 \leq X \leq 1$.

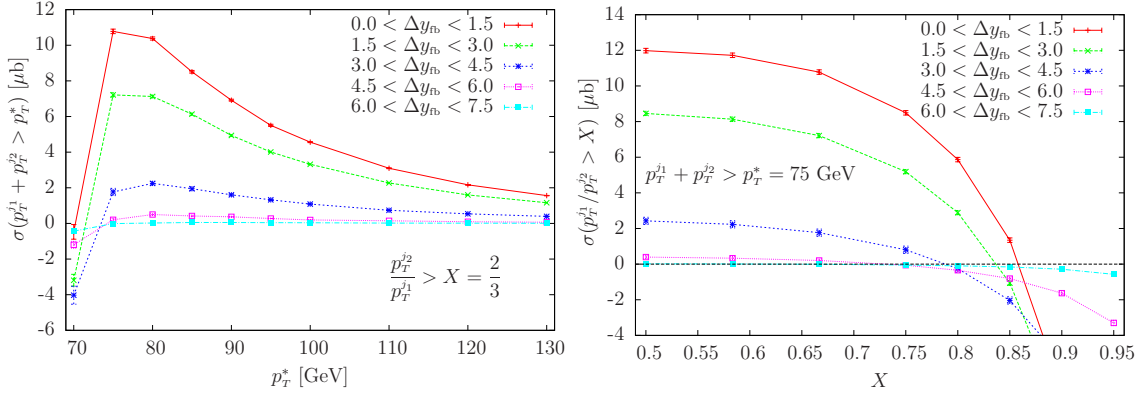


Figure 5: Cross sections for different slices in Δy_{fb} as a function of p_T^* at $X = 2/3$ (left plot) and as a function of X at $p_T^* = 75$ GeV (right plot).

4. Probing higher-order corrections: a comparison among POWHEG, HEJ and NLO results

In the previous section, we investigated various sets of cuts for avoiding regions of the phase space where the fixed NLO calculation becomes unreliable. We are now in a position to compare two theoretical approaches to dijet production that include higher order effects: POWHEG and HEJ. These two approaches are clearly very different in their description of QCD radiation. Nevertheless, for several kinematic distributions (see for example ref. [22]), the predictions from POWHEG and HEJ are very similar. We investigate here a few observables which could expose the differences in the two approaches and we compare them with the fixed NLO results. In order to avoid biasing our event sample, we impose a minimal set of asymmetric cuts

$$p_T^j > 35 \text{ GeV}, \quad p_T^{j1} > 45 \text{ GeV}, \quad |y_j| < 4.7, \quad (4.1)$$

i.e. all jets are required to have a minimum transverse momentum of 35 GeV, and the hardest-jet transverse momentum, p_T^{j1} , is required to be greater than 45 GeV. In order to comply with the experimental acceptance, all jets are further required to have an absolute rapidity $|y_j|$ less than 4.7. Jets are defined according to the anti- k_T jet algorithm, with radius $R = 0.5$. Only events with at least two jets fulfilling eq. (4.1) are kept. We stress that neither the POWHEG nor the HEJ descriptions suffer from using symmetric cuts, since they do a partial resummation of the large logarithmic terms. However, in order to have a sensible fixed NLO cross section to compare with, we impose asymmetric cuts.

In the following, we compare the cross sections computed with a fixed NLO calculation and with HEJ, with the results obtained analyzing 14M events generated by the POWHEG BOX, at the level of the first-emission and after the shower performed by PYTHIA². The renormalization and factorization scales have been chosen equal to the transverse momentum of the hardest jet in each event, for the HEJ predictions. For the NLO computation (and for computing the POWHEG \bar{B} function), scales are set to the transverse momentum of the underlying-Born configuration, as in the previous section. Scale-uncertainty bands,

²We used PYTHIA 6.4.25 with the AMBT1 tune.

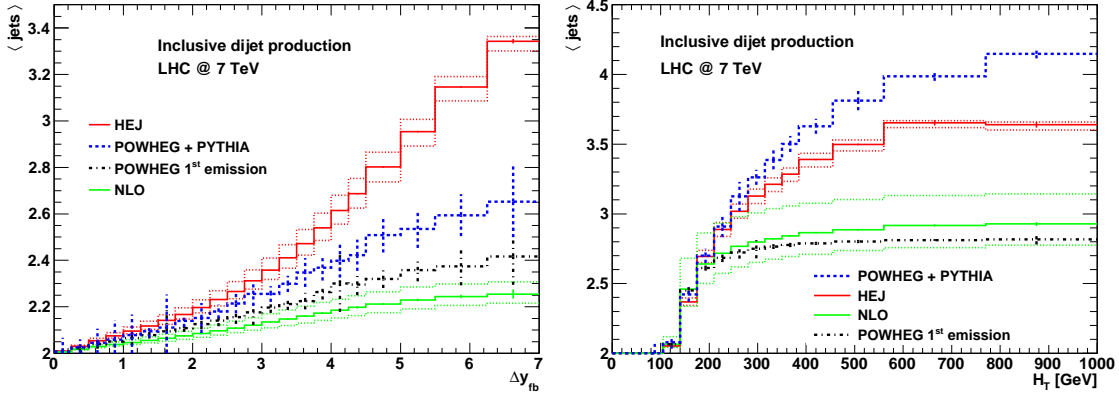


Figure 6: The average number of jets as a function of Δy_{fb} (left plot) and of H_T (right plot), as predicted by a fixed NLO calculation, by POWHEG first emission, by POWHEG+PYTHIA and by HEJ. The dotted red lines around the HEJ prediction and the green ones around the NLO result are obtained by varying the renormalization and factorization scales by a factor of two around their central value.

obtained by varying these scales by a factor of two in each direction, are shown for the NLO and HEJ results. The scales entering in the evaluation of parton distribution functions and of the strong coupling in the POWHEG Sudakov form factor are instead evaluated with a scale equal to the transverse momentum of the POWHEG hardest emission [29, 30].

The statistical errors (due to the numerical integration of the differential cross sections) on the theoretical predictions for the ratios studied in this section have been computed with the standard propagation of errors for the ratio of two uncorrelated quantities. We expect these errors to be an overestimation of the true ones, since, in our case, numerator and denominator are strongly correlated. To have a better estimation of the statistical error, we have applied a different method to the results produced by HEJ: we have divided the 7×10^9 generated events into 13 non-overlapping samples of equal size, and investigated the variation in the determination of the physical distributions of interest, when using all 286 possibilities of choosing groups of 10 sub-samples out of the 13³. The estimate of the statistical fluctuation is determined by requiring that 68% of the results from these samples lies within the upper and lower boundaries. The numbers thus obtained agree well with the estimate obtained by using the standard variance form the same samples.

In fig. 6 we plot the average number of jets as a function of the rapidity difference Δy_{fb} between the most forward and most backward of the jets fulfilling eq. (4.1), on the left, and as a function of $H_T = \sum_j p_T^j$ on the right. The wide-angle resummation implemented in HEJ produces more hard jets than POWHEG and the fixed NLO calculation, as Δy_{fb} increases. Both the NLO and the first-emission POWHEG results have at most 3 jets, so that the average number of jets cannot exceed 3, and are in good agreement. Additional jets are instead

³The numbers 10 and 13 were chosen such that a reasonable convergence was obtained in each group, while maintaining a sufficient number of ways to pick 10 sub-samples for the statistics on the variation to be trustworthy.

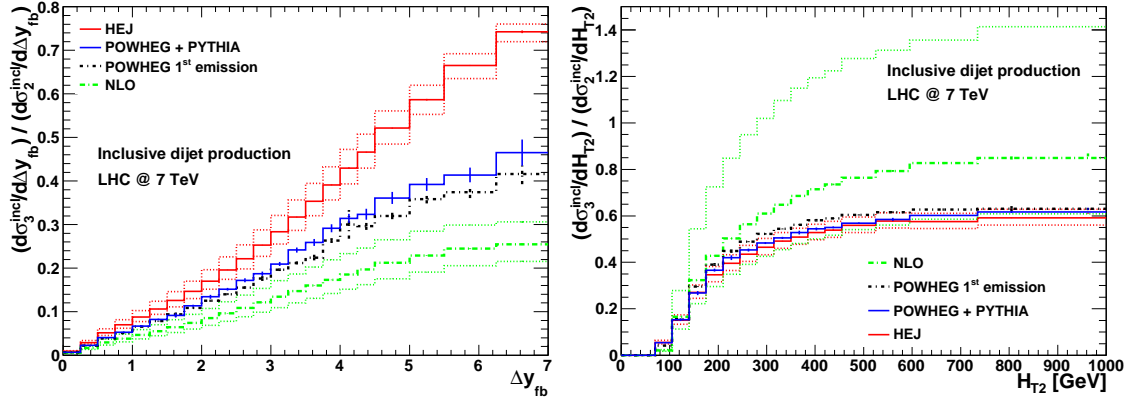


Figure 7: Ratio of the inclusive 3-jet rate over the inclusive 2-jet one, as a function of Δy_{fb} (left plot) and H_{T2} (right plot). The dotted lines display the results obtained by varying the renormalization and factorization scales by a factor of two around the central value, for the HEJ (red) and NLO (green) predictions.

produced by the PYTHIA shower, so that the average number of jets is increased by roughly 20% with respect to the NLO one, for $\Delta y_{fb} \approx 7$. For the same separation in rapidity, the HEJ prediction is 45% larger than the NLO result, with a chance to distinguish among the three approaches. This same distribution has been investigated also in the analysis by ATLAS [22], but, as discussed earlier, the cuts applied in that analysis enhance the effects of collinear emissions, which are treated to leading-logarithmic order in POWHEG and partly in HEJ. In fact, the cuts in eq. (4.1) do not impose a large hierarchy of transverse scales and therefore avoid inducing dominance by collinear-soft emissions. The scale variation (dotted lines around the NLO and HEJ curves) are modest, of the order of a few percent. As a final comment, we note that the prediction from HEJ was found to be very stable against the effects of further showering [41] (using cuts very similar to those in eq. (4.1)).

The dependence of the average number of jets on H_T (right plot) displays a different behaviour: here the showered events have, on average, more jets than HEJ and the NLO results, as the sum of the transverse momentum of all the final-state jets increases. It is interesting here to comment on the NLO result obtained with the factorization and renormalization scales set to $p_T^{UB}/2$, half of the transverse momentum of the underlying-Born configuration, i.e. the upper green dotted line in the plot. In fact, this quantity displays an unphysical behaviour: the average number of jets is greater than 3 for $H_T \gtrsim 270$ GeV. We will comment on this after the discussion of fig. 7, that suffers from the same problem.

In fact, in fig. 7, we plot the ratio of the 3-jet inclusive cross section over the 2-jet one, as a function of Δy_{fb} (left plot) and as a function of H_{T2} (right plot), where $H_{T2} = p_T^{j1} + p_T^{j2}$ is the sum of the transverse momenta of the two hardest jets in the event. The same comments made about the left plot of fig. 6 apply here: the BFKL-inspired resummation implemented by HEJ produces more hard jets than the resummation of the

parton shower of POWHEG+PYTHIA, for large rapidity separation between the most forward and most backward jet. For this distribution, an experimental analysis should then be able to distinguish between the HEJ and the POWHEG+PYTHIA predictions.

In the right plot, the NLO ratio for the 3-jet inclusive cross section over the 2-jet one, plotted as a function of H_{T2} , becomes unphysical (i.e. it gets greater than 1) when the factorization and renormalization scales are set to $p_T^{\text{UB}}/2$, for higher values of H_{T2} . This result is linked with the same unreliable behavior of the NLO distribution in the right plot of fig. 6, and deserves an explanation. For ease of notation we introduce the following shortcuts

$$\tilde{\sigma}_2^{\text{incl}} = \frac{d\sigma_2^{\text{incl}}}{dH_{T2}}, \quad \tilde{\sigma}_3^{\text{incl}} = \frac{d\sigma_3^{\text{incl}}}{dH_{T2}}, \quad (4.2)$$

where the lower index 2 or 3 indicates the number of jets, and the differential cross sections are inclusive with respect to the corresponding number of jets. Together with inclusive cross sections, we define the exclusive ones, that will be designated with the upper label “excl”. At fixed NLO, in dijet production, we have

$$\tilde{\sigma}_3^{\text{incl}} = \tilde{\sigma}_3^{\text{excl}}, \quad \tilde{\sigma}_2^{\text{incl}} = \tilde{\sigma}_2^{\text{excl}} + \tilde{\sigma}_3^{\text{excl}}, \quad (4.3)$$

and we can relate the average number of jets with the inclusive 3-jet over 2-jet ratio

$$\langle \text{jets} \rangle \equiv \frac{2\tilde{\sigma}_2^{\text{excl}} + 3\tilde{\sigma}_3^{\text{excl}}}{\tilde{\sigma}_2^{\text{excl}} + \tilde{\sigma}_3^{\text{excl}}} = 2 + \frac{\tilde{\sigma}_3^{\text{excl}}}{\tilde{\sigma}_2^{\text{incl}}} = 2 + \frac{\tilde{\sigma}_3^{\text{incl}}}{\tilde{\sigma}_2^{\text{incl}}} \quad (4.4)$$

so that the two unphysical behaviors of the right plots in figs. 6 and 7 are strictly connected. The ratio

$$\frac{\tilde{\sigma}_3^{\text{incl}}}{\tilde{\sigma}_2^{\text{incl}}} = \frac{\tilde{\sigma}_3^{\text{incl}}}{\tilde{\sigma}_2^{\text{excl}} + \tilde{\sigma}_3^{\text{incl}}} \quad (4.5)$$

can become greater than 1 for particular kinematic configurations only if the exclusive 2-jet cross section becomes negative at those phase space points. This happens, in our plots, when we choose $p_T^{\text{UB}}/2$ as factorization and renormalization scale, for values of $H_{T2} \gtrsim 270$ GeV. We have explicitly checked that the same behavior is observed if one sets the scale to be the hardest transverse momentum of the NLO partonic kinematics, a scale that is generally used for this kind of process.

In the left plot of fig. 8, we plotted $\tilde{\sigma}_2^{\text{excl}}$, and, as expected, it becomes unphysical when the scale chosen is $p_T^{\text{UB}}/2$ and for values of $H_{T2} \gtrsim 270$ GeV. The explanation of this can be again traced back to the large logarithmic terms related to symmetric cuts and to the increase of the value of α_s , now evaluated at a smaller scale (the rôle played by the factorization scale would be more difficult to disentangle, since it involves the behavior of the parton distribution functions too). The 2-jet exclusive cross section always gets contribution from the Born and the virtual terms, irrespective of the value of H_{T2} , and from the part of the real-emission cross section that, at those kinematic points, is clustered into a 2-jet configuration

$$\tilde{\sigma}_2^{\text{excl}} = \tilde{\sigma}_2^B + \tilde{\sigma}_2^V + \tilde{\sigma}_2^R = \alpha_s^2(\mu) \{ B + \alpha_s(\mu) [V + R_2] \}, \quad (4.6)$$

where the notation is self-explanatory and we put in evidence the appearance of the strong coupling constant $\alpha_s(\mu)$ evaluated at the scale μ . Since B and R_2 are necessarily positive,

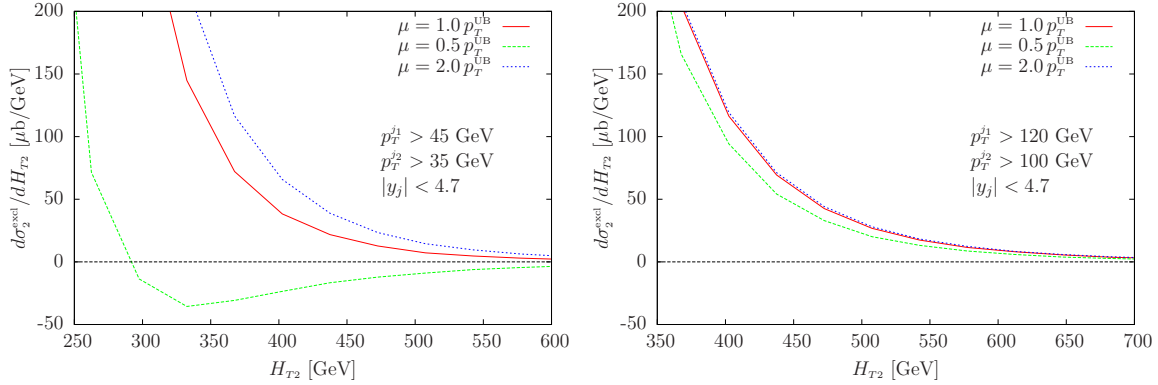


Figure 8: Exclusive 2-jet cross section as a function of H_{T2} , for three values of the renormalization and factorization scale $\mu \{p_T^{\text{UB}}, p_T^{\text{UB}}/2, 2p_T^{\text{UB}}\}$, and for different set of cuts on the minimum-jet p_T .

coming from the square of the respective matrix element, it is the virtual term V that drives $\tilde{\sigma}_2^{\text{excl}}$ to negative values. In other words, the R_2 term becomes smaller and smaller if compared to the absolute value of V . At high values of H_{T2} , most of the events have three jets, with the two hard jets with $p_T \sim H_{T2}/2$, because, most likely, the transverse momentum of the third jet is just high enough to pass the cuts in eq. (4.1). Since the minimum p_T for the jets is 35 GeV, the imbalance between the two hardest jets is small, and the situation is equivalent to imposing symmetric cuts. On the other hand, if we increase to 100 GeV the minimum transverse momentum to define a jet, as in the right plot of fig. 8, the imbalance between the two hardest jet is no longer small compared to their average transverse momentum, and the event kinematics stays away from the symmetric-cut configuration. In addition, we have explicitly checked that, by keeping the p_T cuts of eq. (4.1) but restricting the jet-rapidity range to $|y_j| < 2.5$, the critical H_{T2} value is moved to higher values, i.e. ~ 400 GeV, implying that the unphysical behaviour depends on both the transverse momentum and the rapidity cuts.

Turning now to the predictions from HEJ and POWHEG+PYTHIA in the right plot of fig. 7, we can see that they are in remarkable good agreement, both close to the POWHEG first-emission result, implying that the first POWHEG emission has the strongest impact on this distribution, while the subsequent shower has a milder effect. Before leaving this discussion, we would like to point out that, when using the cuts reported by the ATLAS Collaboration [23]

$$p_T^j > 60 \text{ GeV}, \quad p_T^{j1} > 80 \text{ GeV}, \quad |y_j| < 2.8, \quad (4.7)$$

no significant difference has been found between the NLO result and the other three curves, so that the comparison the ATLAS Collaboration did is meaningful.

As a last example of kinematic distribution that displays different behaviour if evaluated at NLO or using POWHEG or HEJ, we plot, in fig. 9, the average value of $\cos(\pi - \phi_{\text{fb}})$, where ϕ_{fb} is the azimuthal angle between the most forward and backward jets, as a function of their rapidity separation Δy_{fb} . For dijet events at tree-level, $\phi_{\text{fb}} = \pi$, since the two jets are back-to-back, and the average value of the cosine is 1. Deviation from 1 then indicates the presence of additional emissions, so that this kinematic distribution carries

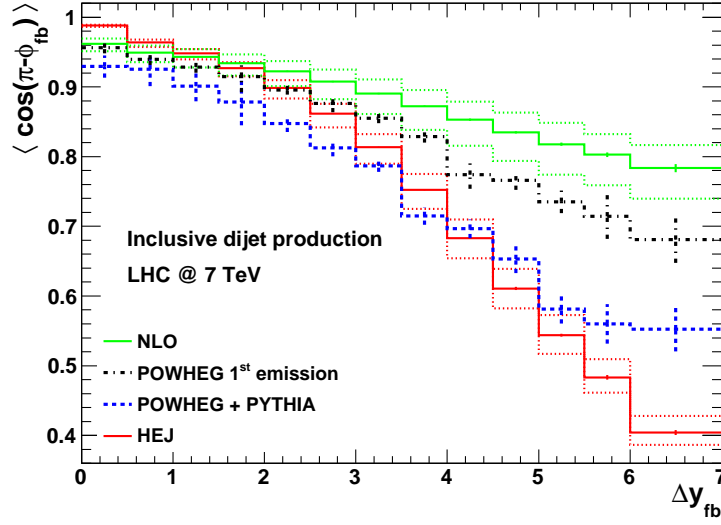


Figure 9: The average value of $\cos(\pi - \phi_{fb})$ as a function of Δy_{fb} , where ϕ_{fb} is the azimuthal angle separation between the most forward and most backward jet. The dotted red and green lines are obtained by varying the renormalization and factorization scales by a factor of 2 in both directions around the central value.

information on the decorrelation between the two jets. This observable has been promoted for a long time as a good discriminator between descriptions with and without a systematic evolution in rapidity. It has therefore also been studied with full detector simulation in ref. [44]. However, the striking prediction from pure leading logarithmic BFKL evolution of an azimuthal decorrelation much larger than that which is obtained in a parton shower or fixed order formulation has been brought into question for some time by the inclusion of subleading corrections [45, 46]. This quantity is more inclusive than the average number of jets as it is sensitive also to emissions below the jet p_T cut. The higher radiation activity in POWHEG+PYTHIA and in HEJ, with respect to the fixed NLO and the POWHEG first-emission results, is clearly visible in the figure: the stronger jet activity produced by HEJ at higher rapidity separation (see the left plot of fig. 6) lowers the average value of the cosine below the POWHEG+PYTHIA result. As expected, the average value predicted by the POWHEG first-emission and the NLO calculation is closer to 1, since they contain at most one radiated parton.

5. Conclusions

Recent analyses by the ATLAS and the CMS Collaborations of inclusive and exclusive dijet production showed a high level of agreement between the two very different approaches to the description of perturbative higher-order corrections implemented in the POWHEG BOX and in HEJ.

Inspired by these results, we have discussed the results obtained using a fixed NLO calculation, HEJ and POWHEG+PYTHIA, in the description of several kinematic distributions,

selected in order to display more clearly the differences among the three approaches: the average number of jets, the ratio of the inclusive three-jet rate over the two-jet one, and the azimuthal decorrelation between the most forward and the most backward jet.

In order to perform a meaningful comparison between the NLO predictions and the resummed results obtained by POWHEG and HEJ, we first investigated the effect of a few sets of cuts, and we discussed which of them do not undermine the convergence of the fixed NLO results. In addition to the commonly used asymmetric cuts, we also considered a slightly different variant of them (the BFKL-inspired cuts of eq. (3.2)). It would be interesting to further explore the usage of these different cuts both theoretically and experimentally.

Then we studied several kinematic distributions where the predictions of POWHEG+PYTHIA and HEJ differ significantly. While the limitations of the NLO calculation are clearly visible when we probe regions of the phase space where multi-jet emissions become important, the predictions of POWHEG+PYTHIA and HEJ are distinguishable when dealing with the average number of jets and the ratio of the inclusive three-jet production over the inclusive two-jet production, when studied as a function of the rapidity separation of the most forward and the most backward jet. Less marked differences are found when these quantities are plotted as a function of the sum of the transverse momenta of all the jets, or as a function of the transverse momenta of the two leading jets. Contrary to these findings, the study of the azimuthal decorrelation of the most forward and backward jet turned out to be less promising in distinguishing the two descriptions given by POWHEG and HEJ.

We hope that an experimental measurement of dijet data collected at the LHC will follow, in order to investigate the quality of the theoretical understanding of these kinematic distributions.

Acknowledgments

The authors would like to thank the staff of the Ecole de Physique des Houches for their hospitality and the organizers of the “Physics at TeV Colliders 2011” workshop held there, where this project was started. We are also grateful for useful discussions with Gavin Salam and the other members of the LPCC Small- x discussion forum on a number of occasions. ER and JMS are supported by the UK Science and Technology Facilities Council (STFC). ER and SA acknowledge financial support from the LHCPhenoNet network under the Grant Agreement PITN-GA-2010-264564 for travel expenses.

References

- [1] V. Del Duca, W. Kilgore, C. Oleari, C. Schmidt, and D. Zeppenfeld, *H + 2 jets via gluon fusion*, *Phys. Rev. Lett.* **87** (2001) 122001, [[hep-ph/0105129](#)].
- [2] V. Del Duca, W. Kilgore, C. Oleari, C. Schmidt, and D. Zeppenfeld, *Gluon-fusion contributions to H + 2 jet production*, *Nucl. Phys.* **B616** (2001) 367–399, [[hep-ph/0108030](#)].
- [3] T. Figy, C. Oleari, and D. Zeppenfeld, *Next-to-leading order jet distributions for Higgs boson production via weak-boson fusion*, *Phys. Rev.* **D68** (2003) 073005, [[hep-ph/0306109](#)].

- [4] V. Ravindran, J. Smith, and W. L. Van Neerven, *Next-to-leading order QCD corrections to differential distributions of Higgs boson production in hadron hadron collisions*, *Nucl. Phys.* **B634** (2002) 247–290, [[hep-ph/0201114](#)].
- [5] E. L. Berger and J. M. Campbell, *Higgs boson production in weak boson fusion at next-to-leading order*, *Phys. Rev.* **D70** (2004) 073011, [[hep-ph/0403194](#)].
- [6] T. Plehn, D. L. Rainwater, and D. Zeppenfeld, *Determining the structure of Higgs couplings at the LHC*, *Phys. Rev. Lett.* **88** (2002) 051801, [[hep-ph/0105325](#)].
- [7] G. Klamke and D. Zeppenfeld, *Higgs plus two jet production via gluon fusion as a signal at the CERN LHC*, *JHEP* **0704** (2007) 052, [[hep-ph/0703202](#)].
- [8] Y. L. Dokshitzer, V. A. Khoze, and T. Sjostrand, *Rapidity gaps in Higgs production*, *Phys. Lett.* **B274** (1992) 116–121.
- [9] V. Del Duca, A. Frizzo, and F. Maltoni, *Higgs boson production in association with three jets*, *JHEP* **05** (2004) 064, [[hep-ph/0404013](#)].
- [10] V. Del Duca *et. al.*, *Monte Carlo studies of the jet activity in Higgs + 2 jet events*, *JHEP* **10** (2006) 016, [[hep-ph/0608158](#)].
- [11] J. M. Campbell, R. K. Ellis, and G. Zanderighi, *Next-to-leading order Higgs + 2 jet production via gluon fusion*, *JHEP* **10** (2006) 028, [[hep-ph/0608194](#)].
- [12] J. M. Campbell, R. Ellis, and C. Williams, *Hadronic production of a Higgs boson and two jets at next-to-leading order*, *Phys. Rev.* **D81** (2010) 074023, [[arXiv:1001.4495](#)].
- [13] SM and NLO Multileg Working Group Collaboration, J. R. Andersen *et. al.*, *The SM and NLO multileg working group: Summary report*, [arXiv:1003.1241](#).
- [14] V. Del Duca, W. Kilgore, C. Oleari, C. R. Schmidt, and D. Zeppenfeld, *Kinematical limits on Higgs boson production via gluon fusion in association with jets*, *Phys. Rev.* **D67** (2003) 073003, [[hep-ph/0301013](#)].
- [15] J. R. Andersen and C. D. White, *A New Framework for Multijet Predictions and its application to Higgs Boson production at the LHC*, *Phys. Rev.* **D78** (2008) 051501, [[arXiv:0802.2858](#)].
- [16] J. R. Andersen, V. Del Duca, and C. D. White, *Higgs Boson Production in Association with Multiple Hard Jets*, *JHEP* **02** (2009) 015, [[arXiv:0808.3696](#)].
- [17] J. R. Andersen, K. Arnold, and D. Zeppenfeld, *Azimuthal Angle Correlations for Higgs Boson plus Multi- Jet Events*, *JHEP* **06** (2010) 091, [[arXiv:1001.3822](#)].
- [18] V. S. Fadin, E. A. Kuraev, and L. N. Lipatov, *On the Pommeranchuk singularity in asymptotically free theories*, *Phys. Lett.* **B60** (1975) 50–52.
- [19] E. A. Kuraev, L. N. Lipatov, and V. S. Fadin, *Multi-Reggeon processes in the Yang-Mills theory*, *Sov. Phys. JETP* **44** (1976) 443–450.
- [20] E. A. Kuraev, L. N. Lipatov, and V. S. Fadin, *The Pommeranchuk singularity in nonabelian gauge theories*, *Sov. Phys. JETP* **45** (1977) 199–204.
- [21] I. I. Balitsky and L. N. Lipatov, *The Pommeranchuk singularity in quantum chromodynamics*, *Sov. J. Nucl. Phys.* **28** (1978) 822–829.

- [22] **ATLAS Collaboration** Collaboration, G. Aad *et. al.*, *Measurement of dijet production with a veto on additional central jet activity in pp collisions at $\sqrt{s} = 7$ TeV using the ATLAS detector*, *JHEP* **1109** (2011) 053, [[arXiv:1107.1641](#)].
- [23] **ATLAS Collaboration** Collaboration, G. Aad *et. al.*, *Measurement of multi-jet cross sections in proton-proton collisions at a 7 TeV center-of-mass energy*, *Eur.Phys.J.* **C71** (2011) 1763, [[arXiv:1107.2092](#)].
- [24] **ATLAS Collaboration** Collaboration, G. Aad *et. al.*, *Measurement of inclusive jet and dijet production in pp collisions at $\sqrt{s} = 7$ TeV using the ATLAS detector*, [arXiv:1112.6297](#).
- [25] **CMS Collaboration**, S. Chatrchyan *et. al.*, *Measurement of the Ratio of the 3-jet to 2-jet Cross Sections in pp Collisions at $\sqrt{s} = 7$ TeV*, *Phys.Lett.* **B702** (2011) 336–354, [[arXiv:1106.0647](#)].
- [26] **CMS Collaboration**, V. Khachatryan *et. al.*, *Dijet Azimuthal Decorrelations in pp Collisions at $\sqrt{s} = 7$ TeV*, *Phys.Rev.Lett.* **106** (2011) 122003, [[arXiv:1101.5029](#)].
- [27] **CMS Collaboration**, S. Chatrchyan *et. al.*, *Measurement of the inclusive production cross sections for forward jets and for dijet events with one forward and one central jet in pp collisions at $\sqrt{s} = 7$ TeV*, [arXiv:1202.0704](#).
- [28] P. Nason, *A New method for combining NLO QCD with shower Monte Carlo algorithms*, *JHEP* **0411** (2004) 040, [[hep-ph/0409146](#)].
- [29] S. Frixione, P. Nason, and C. Oleari, *Matching NLO QCD computations with Parton Shower simulations: the POWHEG method*, *JHEP* **0711** (2007) 070, [[arXiv:0709.2092](#)].
- [30] S. Alioli, K. Hamilton, P. Nason, C. Oleari, and E. Re, *Jet pair production in POWHEG*, *JHEP* **1104** (2011) 081, [[arXiv:1012.3380](#)].
- [31] J. R. Andersen and J. M. Smillie, *Constructing All-Order Corrections to Multi-Jet Rates*, *JHEP* **1001** (2010) 039, [[arXiv:0908.2786](#)].
- [32] J. R. Andersen and J. M. Smillie, *The Factorisation of the t-channel Pole in Quark-Gluon Scattering*, *Phys.Rev.* **D81** (2010) 114021, [[arXiv:0910.5113](#)].
- [33] J. R. Andersen and J. M. Smillie, *Multiple Jets at the LHC with High Energy Jets*, *JHEP* **1106** (2011) 010, [[arXiv:1101.5394](#)].
- [34] S. Alioli, P. Nason, C. Oleari, and E. Re, *A general framework for implementing NLO calculations in shower Monte Carlo programs: the POWHEG BOX*, *JHEP* **1006** (2010) 043, [[arXiv:1002.2581](#)].
- [35] T. Sjostrand, S. Mrenna, and P. Z. Skands, *PYTHIA 6.4 Physics and Manual*, *JHEP* **0605** (2006) 026, [[hep-ph/0603175](#)].
- [36] J. Alwall *et. al.*, *MadGraph/MadEvent v4: The New Web Generation*, *JHEP* **09** (2007) 028, [[arXiv:0706.2334](#)].
- [37] S. Frixione and G. Ridolfi, *Jet photoproduction at HERA*, *Nucl. Phys.* **B507** (1997) 315, [[hep-ph/9707345](#)].
- [38] J. R. Andersen, V. Del Duca, S. Frixione, C. R. Schmidt, and W. J. Stirling, *Mueller-Navelet jets at hadron colliders*, *JHEP* **02** (2001) 007, [[hep-ph/0101180](#)].
- [39] A. Banfi and M. Dasgupta, *Dijet rates with symmetric E_t cuts*, *JHEP* **01** (2004) 027, [[hep-ph/0312108](#)].

- [40] M. Cacciari, G. P. Salam, and G. Soyez, *The Anti- k_t jet clustering algorithm*, *JHEP* **0804** (2008) 063, [[arXiv:0802.1189](#)].
- [41] J. R. Andersen, L. Lönnblad, and J. M. Smillie, *A Parton Shower for High Energy Jets*, *JHEP* **1107** (2011) 110, [[arXiv:1104.1316](#)].
- [42] M. Klasen and G. Kramer, *Dijet cross-sections at $\mathcal{O}(\alpha_s^2)$ in photon-proton collisions*, *Phys.Lett.* **B366** (1996) 385–393, [[hep-ph/9508337](#)].
- [43] A. D. Martin, W. J. Stirling, R. S. Thorne, and G. Watt, *Parton distributions for the LHC*, *Eur. Phys. J.* **C63** (2009) 189–285, [[arXiv:0901.0002](#)].
- [44] D. d’Enterria, *Forward jets physics in ATLAS, CMS and LHCb*, [arXiv:0911.1273](#).
- [45] L. H. Orr and W. J. Stirling, *Dijet production at hadron hadron colliders in the BFKL approach*, *Phys. Rev.* **D56** (1997) 5875–5884, [[hep-ph/9706529](#)].
- [46] D. Colferai, F. Schwennsen, L. Szymanowski, and S. Wallon, *Mueller Navelet jets at LHC - complete NLL BFKL calculation*, *JHEP* **1012** (2010) 026, [[arXiv:1002.1365](#)].